Journal of Nuclear Materials 381 (2008) 76–82

Contents lists available at ScienceDirect

Journal of Nuclear Materials

journal homepage: www.elsevier.com/locate/jnucmat

Accumulation of thermal resistance in neutron irradiated graphite materials

L.L. Snead

Materials Science and Technology Division, Oak Ridge National Laboratory, UT-Battele, P.O. Box 2008, Oak Ridge, TN 37831, United States

A B S T R A C T

A nuclear graphite, H451, and two high thermal conductivity graphite composites have been irradiated in the temperature range of 310–710 °C in the high flux isotope reactor and their thermal conductivities monitored in situ. Data were measured continuously up to a fast neutron dose of approximately 1×10^{25} n/m^2 ($E > 0.1$ MeV). Data are interpreted in terms of the added thermal resistance and materials compared on this basis. Following this analysis it is shown that for the three materials studied, which have significantly different initial thermal conductivity values, the accumulation of thermal resistance is greater for the materials with lower initial thermal conductivity. Given that vacancies dominate phonon scattering at these irradiation temperatures and dose levels, these data clearly indicate that materials of higher perfection have a slower rate of stable vacancy accumulation during irradiation.

Published by Elsevier B.V.

1. Introduction

The physical processes governing the thermal conductivity of graphite, as well as the mechanisms responsible for the radiation-induced degradation in thermal conductivity, have been well established [1,2]. For all but the poorest grades of carbon, thermal conductivity is dominated by phonon transport along the graphite basal planes and is reduced by scattering obstacles such as grain boundaries, lattice defects, inclusions, and composite interfaces. For graphite with the largest crystallites, i.e. pyrolytic or natural flake graphite, the in-plane room temperature thermal conductivity approaches 2000 W/m-K [3]. The same mechanisms governing intrinsic and radiation-degraded thermal conductivity of graphite hold true for carbon–carbon composites.

The thermal conductivity of graphite-based materials can be written as a summation of the thermal resistances due to scattering obstacles [1,4]:

$$K(x,T) = \alpha(x) \cdot (1/K_u + 1/K_{GB} + 1/K_{RD})^{-1}, \quad (1)$$

where the term $\alpha(x)$ is a coefficient which includes terms due to orientation (with respect to the basal plane or composite orientation (x)), porosity and some other minor contributors. The first two terms inside the parentheses are the contributions to the thermal conductivity due to the Umklapp scattering ($1/K_u$) and the grain boundary scattering ($1/K_{GB}$), respectively. The grain boundary phonon scattering ($1/K_{GB}$) dominates thermal resistance at low-temperatures and is insignificant above a few hundred degrees Celsius, depending on the perfection of the graphite. For the irradiation temperature of this study (>310 °C), the grain boundary term can therefore be neglected. Umklapp scattering, or phonon–phonon scattering, dominates thermal conductivity at higher temperatures and scales nearly as T^2 [2]. The Umklapp scattering therefore defines the upper limit in thermal conductivity for 'perfect', non-irradiated, graphite. Following Taylor's analysis [5] the Umklapp-limited thermal conductivity of the graphite crystal is ~2200 W/m-K at room temperature, which is not far removed from the best pyrolytic graphite and vapor grown carbon fibers. For later comparison, the Umklapp thermal resistance ($1/K_u$) at 310 and 710 °C is 0.0012 and 0.0019 m-K/W, respectively.

The third term in Eq. (1), K_{RD}, is the contribution to the thermal resistance in the basal plane due to defect scattering. Following neutron irradiation, various types of stable defects will be produced depending on the irradiation temperature. These defects are very effective in scattering phonons, and in practical terms for nuclear application of graphite quickly becomes the dominant term in Eq. (1). While many types of defects have been identified in graphite, at irradiation temperatures less than ~650 °C, only simple defects are found in significant quantities. It has been further shown [6] that at an irradiation temperature near 150 °C, the defect which dominates the thermal resistance is the single lattice vacancy. For temperatures from ~150 to 1000 °C small vacancy loops also become important. Kelly attributes all thermal conductivity degradation to vacancy and small interstitial complexes for irradiation temperatures less than 650 °C [1,7]. Of significance is that the number of vacancies surviving for a given neutron irradiation dose is a strong function of irradiation temperature, with greater vacancies surviving at lower irradiation temperatures. This is in part the reason why thermal conductivity degradation is greater for low-temperature irradiation.

E-mail address: sneadll@ornl.gov

0022-3115/$ - see front matter Published by Elsevier B.V.
doi:10.1016/j.jnucmat.2008.07.017

It is worth noting that even for the maximum dose of the present study (about 2 displacements per atom; dpa) the material was undergoing volumetric shrinkage [8–10]. At several times the dose of this study both graphite and graphite fiber composite would move into a swelling phase leading to significant disruption of grain boundaries and composite fiber interfaces. For materials entering into the phase of volumetric expansion Eq. (1) would be difficult to apply due to scattering at newly created internal interfaces. This is not the case for the data of this paper as only minimal change in the internal interfaces of these materials are expected.

There have been a few studies aimed at developing dose-temperature algorithms for thermal conductivity degradation of carbon fiber composites and graphite utilizing semi-empirical approaches [11–13]. Numerous algorithms based on particular graphite data have also been generated for specific reactor applications. However, these algorithms had limited basis in the physics of phonon scattering and added little into the physical insight of the processes involved. Their primary purpose was to provide tools to reactor designers and in that way proved useful. Moreover, standard practice for comparing irradiation performance of various grades of graphite has been to report thermal conductivity normalized to non-irradiated conductivity. In the early graphite literature an example of this is the work of Kelly [6,14] on pyrolytic graphite, where the metric for comparing the effect of irradiation temperature on conductivity was the 'fractional change in thermal resistance', defined as $(K_{\text{non-irr}}/K_{\text{i}})-1$. Similarly, Burchell uses [15] 'fractional reduction in thermal conductivity', defined as $1-(K_{\text{non-irr}}/K_{\text{i}})$. Both of these simple metrics have been effectively used to compare irradiation effects in one graphite type, or among very similar materials. Over the past decade it has become common practice to compare the degradation of various graphite and composite materials as a ratio of the irradiated to non-irradiated values, $K_{\text{i}}/K_{\text{non-irr}}$ [16–19].

Recently, a variant of the simple metrics discussed above, based on Eq. (1), has been applied to a number of ceramic materials. Specifically, Snead [20] discusses a 'thermal defect resistance approach' to compare the efficiency of neutron irradiation in degrading thermal conductivity of dissimilar ceramics and similar ceramics with a range in thermal conductivity. The thermal defect resistance term is simply found by combining the Umklapp and grain boundary phonon scattering terms of Eq. (1) (yielding $1/K_{\text{non-irr}}$) and solving for the irradiation-induced term $1/K_{\text{RD}}$. In this way it was shown (for monolithic ceramics [20]) that the accumulation of thermal defect resistance ($1/K_{\text{RD}}$) at low neutron dose does not scale proportionally for many ceramics for 60 °C neutron irradiation (in other words the ratio of the change in thermal resistance to the change in neutron fluence is less than unity). This implies significant defect mobility and vacancy annihilation for irradiation near room temperature. Moreover, it was shown that the accumulation of thermal defect resistance for similar materials (e.g., sapphire and high-purity polycrystalline alumina) was similar even though the non-irradiated conductivities were significantly different. This last finding suggests that by mapping the thermal defect resistance for a specific material, such as alumina, the thermal conductivity as a function of irradiation temperature and neutron dose can be predicted for any high-quality alumina independent of the non-irradiated thermal conductivity.

The purpose of this paper is to apply the simple thermal defect resistance approach to a few graphite materials of differing initial thermal conductivities to determine the predictive capability of this method, and to gain insight into the accumulation rate of phonon scattering defects in graphite materials as a function of neutron dose and irradiation temperature.

2. Experimental

Materials for this study (see Table 1) include a nuclear graphite and two high-quality carbon fiber composites. The nuclear graphite was the near-isotropic, medium grain sized (H-451) previously manufactured by Sigri Great Lakes Carbon. The carbon fiber composites were manufactured by Fiber Materials Incorporated (FMI-222) and Mitsubishi Kasei (MKC-1PH). The FMI-222 material is a three-dimensional balanced weave composite utilizing P-55 pitch based fibers and a mesophase pitch matrix. The thermal properties of this composite are isotropic. The MKC-1PH is also based on a pitch fiber (K-139) and a mesophase pitch matrix, though has a one-dimensional architecture yielding highly anisotropic thermal properties. The MKC-1PH was studied in the high conductivity direction only. Fig. 1 gives a plot of thermal conductivity as a function of temperature (in the high conductivity direction where applicable) for the three materials.

Table 1
Properties of material studied

Designation	Manufacturer	Architecture	Constituents	Grain or cell size	Density (g/cc)
H451	Great lakes carbon	graphite	Coal tar pitch binder. Petroleum pitch impregnation. Petroleum coke		1.76
FMI-222	Fiber materials incorporated	3-D balanced weave composite	Amoco P-series pitch fiber. Pitch derived matrix		1.96
MKC-1PH	Mitsubishi Kasei	1-D composite	K-139 pitch based fiber, pitch derived matrix	n/a	1.93

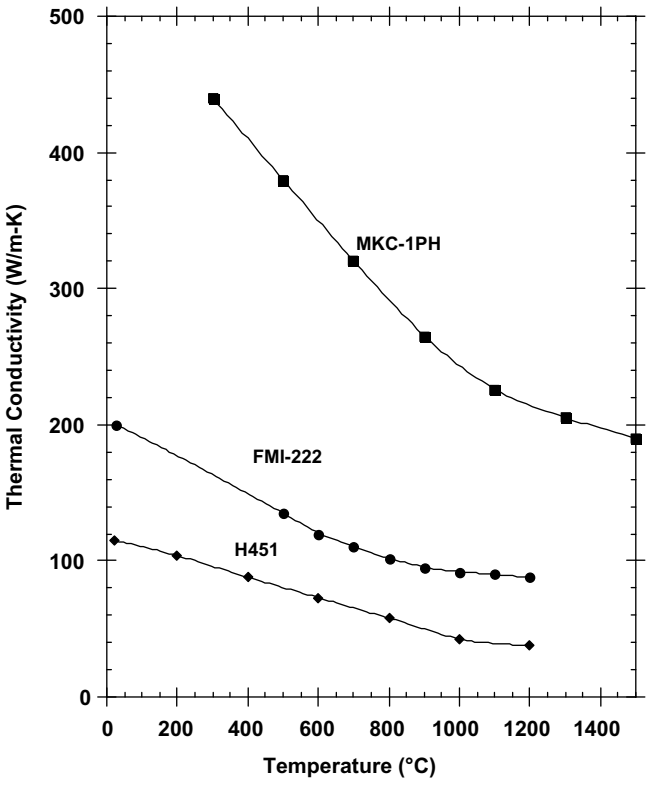

Fig. 1. Non-irradiated thermal conductivity as a function of temperature.

Cylindrical samples were machined from the graphite materials to a diameter of 6 mm and 12 mm length. Following machining shallow pilot holes were drilled 0.76 mm deep into the center of both ends of the sample and one end was brazed to a vanadium heat sink. Very small (0.5 mm) stainless steel sheathed Type N thermocouples were brazed into the pilot holes. A representation of a single vanadium heat sink including two mock samples is given in Fig. 2. Holders were then stacked within a cylindrical aluminum tube, cleaned, and baked at 200 °C in vacuum to drive off moisture. The tube was then filled with a high-purity helium cover gas and welded shut.

Irradiation was carried out in the Removable Beryllium position of the high flux isotope reactor. The peak flux for this position is approximately 6×10^{18} n/m^2-s ($E > 0.1$ MeV). A high-purity variable sweep gas mixture of argon and helium, along with a gas gap between the heat-sink and the aluminum holder, defined the irradiation temperature of the sample. In addition to the thermocouples bonded to the samples, thermocouples were bonded to each heat sink and monitored continuously. These thermocouples were used to continuously vary the argon/helium sweep gas to maintain constant heat sink temperature. The basic concept of this experiment is to constrain the nuclear heat generated within the cylindrical sample to one-dimensional heat flow along the axis of the sample into the heat sink. The gamma heating intrinsic to the reactor core provides the uniform volumetric heat source to the sample. With this technique there are two ways the thermal conductivity can be found. The most straightforward is to use the gamma heating, sample density, distance between thermocouple junctions, and the measured temperature difference between the thermocouples (about 30 °C). A three-dimensional finite element heat transport code was used to incorporate end effects and the presence of the thermocouples. This method yielded a reasonable approximation for thermal conductivity for the samples. A simple 1 one-dimensional heat flow calculation also agreed well with the three-dimensional calculation. However, an error caused by uncertainty in the local gamma heating (possibly significant) and the distance between thermocouples (small) is additive and unknown. For this reason a more straightforward method for calculating thermal conductivity was selected. Specifically, the thermal conductivity as a function of temperature of each sample was measured prior to capsule assembly. The thermal conductivity at the start of the irradiation period was assumed to be the same as the pre-irradiation value and thus fixed. With this assumption the thermal conductivity as a function of time in reactor is inferred directly from the change in the temperature difference between the paired (hot-side and cold-side) sample thermocouples. Implied in this assumption is that gamma heating remained constant throughout the period of irradiation. The operating performance of the high flux isotope reactor, as seen in numerous instrumented capsules, suggests both reactor power and gamma heat flux are constant as a function of core life. The reactor power was extremely constant throughout this particular experiment.

3. Results

The in situ thermal conductivity, measured as a function of time in the HFIR core, is shown in Figs. 3–5. In these figures data are plotted every 15 min though was recorded at a much greater rate. Approximately 524 h into the irradiation a data discontinuity is observed. This discontinuity marks the end of one cycle and the start of the following cycle. The period of refueling between cycles was approximately one week and is omitted from the plot. In Fig. 3 the degradation of H451 thermal conductivity for irradiation temperatures of 430 and 710 °C is provided. These irradiation temperatures are mean values of the hot-side and cold-side thermocouples at the middle of the irradiation period. As the irradiation progressed the temperature difference between the thermocouples increased by as much at 20 °C (due to the degrading thermal conductivity). Considering this along with the small change in temperature between the braze joint and the hot-side thermocouple, the irradiation temperatures quoted from here forward are considered approximations within ~30 °C. From Fig. 3, it is clearly seen that the lower temperature irradiated graphite (430 °C) begins irradiation at a higher value of thermal conductivity though rapidly degrades such that its thermal conductivity is less than the H451 material irradiated at 710 °C. By the end of 1000 h of irradiation the thermal conductivity of the H451 irradiated at 430 °C has been reduced from

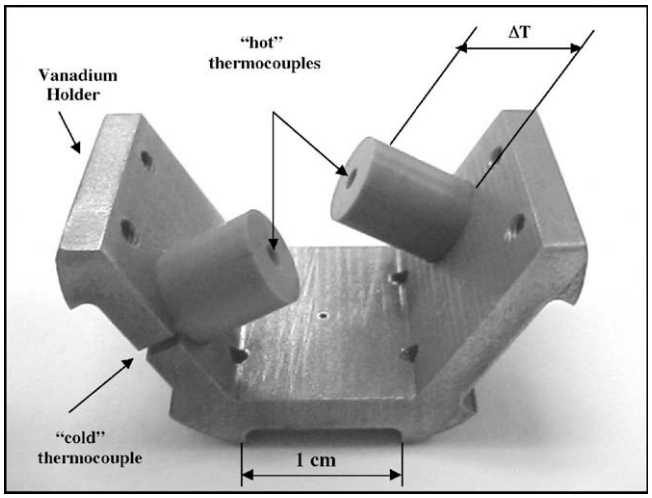

Fig. 2. Mock-up of samples bonded to vanadium heat sink.

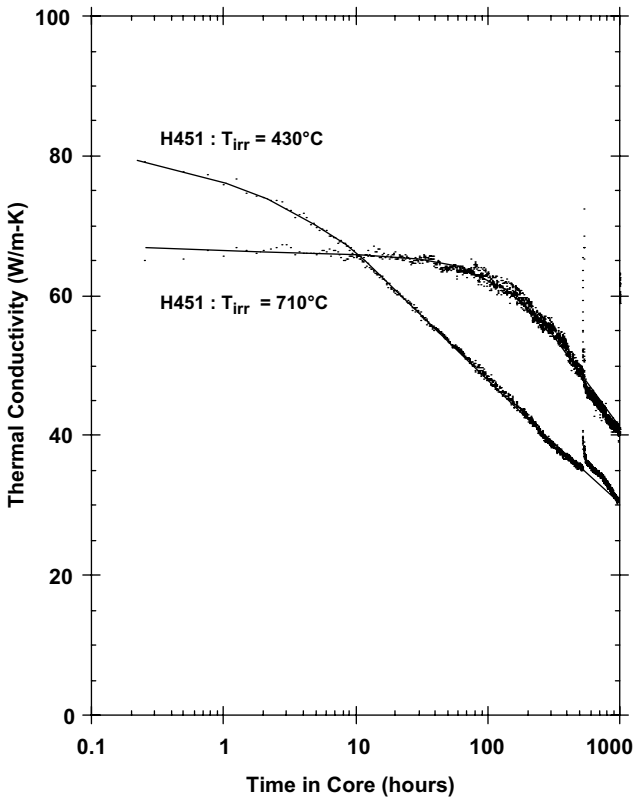

Fig. 3. Thermal conductivity reduction of H451 graphite.

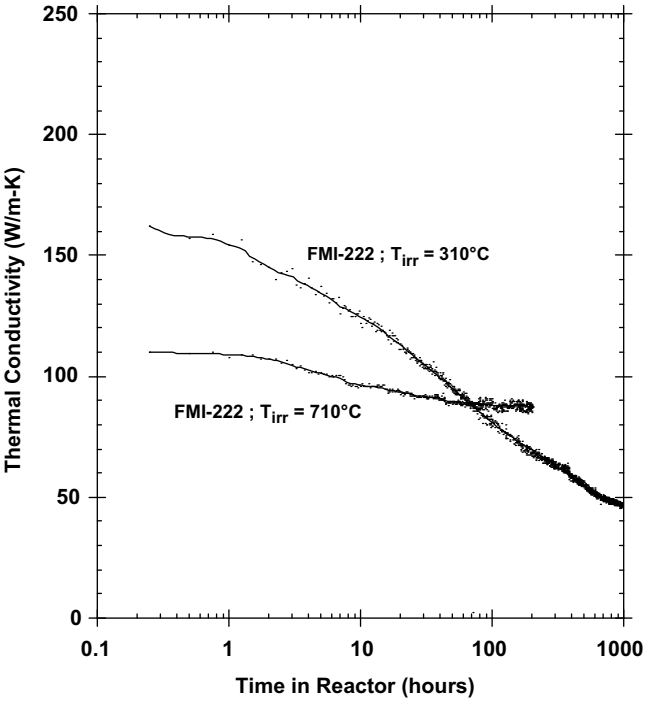

Fig. 4. Thermal conductivity reduction of FMI-222.

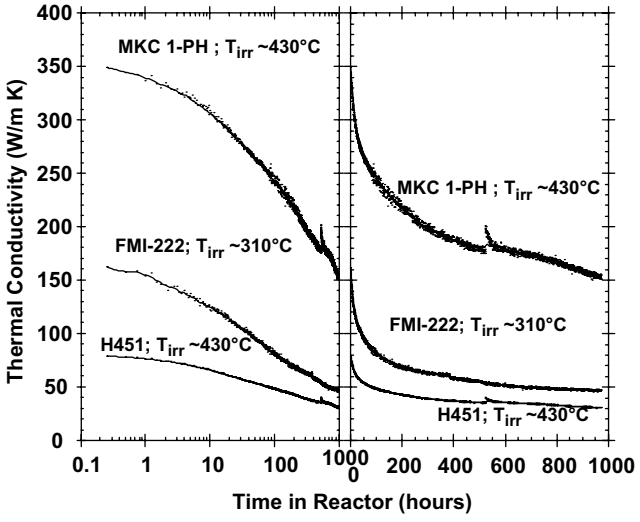

Fig. 5. Thermal conductivity reduction of materials irradiated at 310–430 °C.

~80 to ~30 W/m-K while the sample irradiated at 710 °C has been reduced from about 65 to 40 W/m-K.

An experimental artifact of this work was thermocouple failure. While it is easily shown that thermocouple de-calibration due to nuclear transmutations would not become significant for several cycles, outright thermocouple failure did occur. This failure was presumably due to failure of the magnesium oxide insulation between the thermocouple wires and the thermocouple sheath. This failure is attributed to the extremely small insulating gap required for these 0.5 mm diameter sheathed thermocouples. Thermocouple deterioration and failure, which occurred for about 30% of thermocouples, occurred rapidly, and was preceded by a period of noisy data. An example of this is shown for the 710 °C irradiated FMI-222 composite of Fig. 4 at approximately 200 h into the irradiation. Prior to complete thermocouple failure the data is observed to become noisier. After this point the data was considered unreliable and is left off the plot. In some cases outright failure of the thermocouple attributed to shorting of the thermocouple to the outer sheath occurred.

The data of Fig. 5 gives a relative comparison of the reduction in thermal conductivity for the materials studied at irradiation temperatures of 310–430 °C. It is noted that for 1000 h in core the total displacement dose to these materials was approximately 2×10^{25} n/m^2 ($E > 0.1$ MeV.) The maximum dose of this study does not quite reach thermal conductivity saturation. However, by inspection of the rightmost curve of Fig. 5, which gives the same data plotted on a linear time scale, saturation thermal conductivity has nearly been achieved.

4. Discussion

Unfortunately, ex situ (post-irradiation) thermal conductivity data to precisely compare to results of this work do not exist. However, similar dose and irradiation temperature data do exist for the H451 graphite. In comparison to the data of Fig. 3, Price [21] carried out H451 irradiation at 600 °C which resulted in a thermal conductivity reduction at the irradiation temperature from ~75 (non-irradiated) to ~32 W/m-K for a dose of 2.2×10^{25} n/m^2 ($E > 0.18$ MeV). This is about twice the highest dose of this study and is in general agreement with the extrapolated values of the 430 and 710 °C data of Fig. 3. Engle [22] derives a set of thermal conductivity curves for H451 as a function of dose and irradiation temperature. Extrapolating the Engle data to the 710 °C thermal conductivity curve of Fig. 3, the data corresponding to 100 h in core is ~65 W/m-K while the 1000 h value is ~42 W/m-K. Both of these values are in agreement with the 710 °C curve of Fig. 3. There is very limited data for the composite materials, though Burchell's [15] data on FMI-222 thermal conductivity degradation for an ~600 °C irradiation to twice the dose of the present study are in general agreement with the extrapolated data of Fig. 4. The unidirectional composite MCK-1PH was irradiated by Bonal [18] at the same temperature of this study. His measured thermal conductivity for the irradiation dose of 1.1×10^{25} n/m^2 ($E > 0.1$ MeV) was 120 W/m-K, which is consistent with the extrapolated MKC-1PH data of Fig. 5.

The data on thermal conductivity reduction plotted in Figs. 3–5 indicate an approximately linear degradation of thermal conductivity as a function of log time. This is the case for all but the first few hours of irradiation. All data from this study are replotted in terms of thermal defect resistance in Figs. 6–8. In Fig. 6, the build-up of thermal defect resistance ($1/K_i$, assuming α of unity) for the nuclear graphite H451 is depicted for irradiation temperatures of 430 and 710 °C. At 430 °C a rapid increase followed by a leveling of to an apparently constant accumulation rate. In contrast, the H451 irradiated at 710 °C has a lower accumulation of thermal defect resistance and enters into the linear accumulation regime more rapidly. It is interesting to note that the levels of thermal defect resistance for both irradiation temperatures quickly dominate the thermal resistance due to phonon scattering. As discussed previously, the Umklapp thermal resistance is 0.0012 and 0.0019 at 300 and 700 °C, respectively. The equivalent thermal defect resistance occurs just a few hours into irradiation for H451 irradiated at 300 °C and at about 200 h in reactor for the H451 irradiated at 700 °C.

Fig. 7 gives the thermal defect resistance for the FMI-222 composite irradiated at 310 and 710 °C. As with the lower temperature irradiated H451 graphite, the 310 °C irradiated FMI-222 composite exhibits a sharp initial rise in thermal defect resistance followed by a gradual decline into a linear accumulation regime. Unlike H451

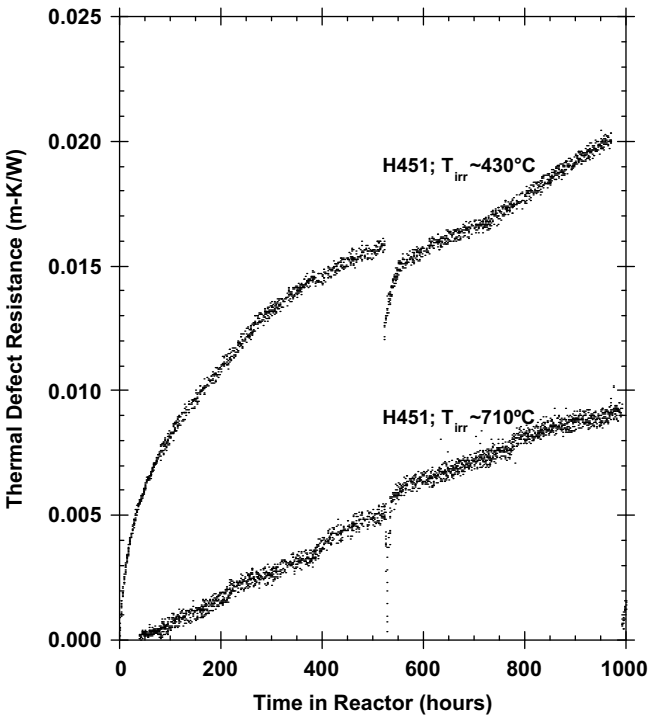

Fig. 6. Accumulated thermal defect resistance of H451.

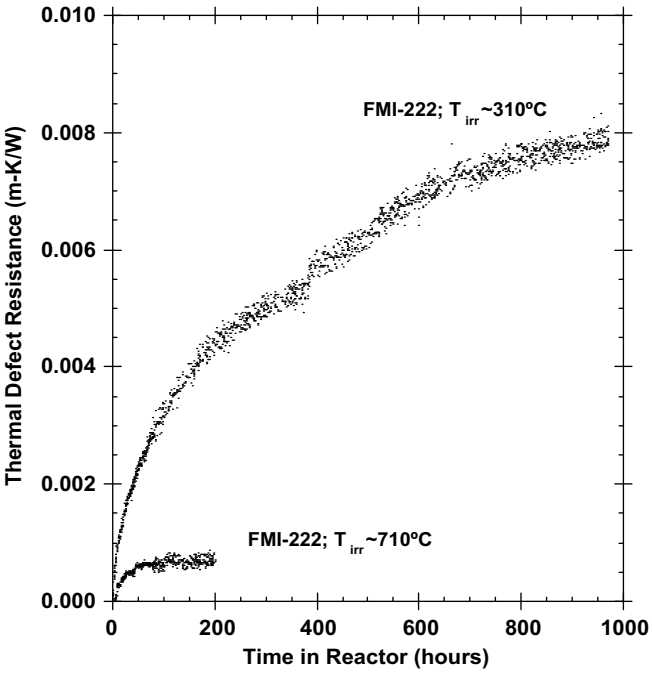

Fig. 7. Accumulated thermal defect resistance of FMI-222.

irradiated at 710 °C, the FMI-222 also exhibits an initial sharp increase. Unfortunately, the data for the FMI-222, 710 °C at >200 h becomes noisy and cannot be used to determine the behavior in the linear accumulation regime.

Of interest in comparing the curves of Figs. 6 and 7 are the relative levels of thermal defect resistance accumulation for the two

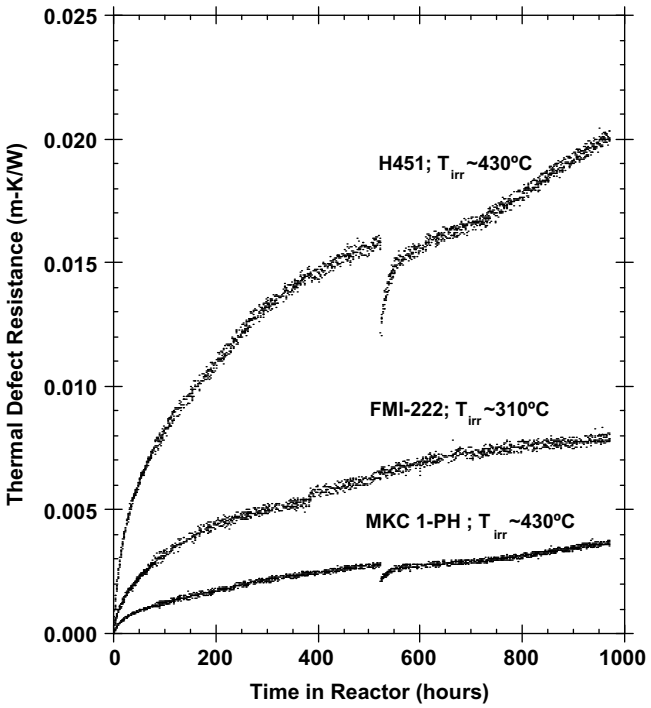

Fig. 8. Comparison of thermal defect resistance for materials irradiated at 310–430 °C.

materials. A straightforward comparison is complicated due to the difference in irradiation temperatures (i.e., 310–430 °C at the low end of the irradiation temperatures), though it is clear that the accumulation rate is substantially higher for the H451 graphite even when considering the differing irradiation temperatures. This point is reinforced by inspection of Fig. 8, which gives a comparison of the low-temperature irradiations for all three materials of this study. Clearly, the magnitude of the initial rise in thermal defect resistance is greater for the lower thermal conductivity materials. The thermal defect accumulation rate of the linear accumulation regime is difficult to compare, though from the data presented in Fig. 8 there appears to be a weak dependence of the accumulation rate on the material. It appears as if there may be a tendency for the lower thermal conductivity materials to have a somewhat higher linear accumulation rate (the slope of the right side of the curves of Fig. 8).

An obvious benefit from generating thermal conductivity data in the manner of this work (in-situ) is the large number of data points taken on a single sample. However, by analyzing literature data from post-irradiation measurement of thermal conductivity the same basic trends discussed in the previous paragraphs are observed. [16,17,19] As example, Wu [17] has reported on thermal conductivity reduction for a range of graphite materials irradiated at temperatures similar to the present study. The Wu data span three decades of fluence corresponding to about 30 min to a few days of irradiation in the present work. By plotting the Wu data in terms of thermal defect resistance the initial build-up, and the transition to a lower accumulation rate, is clearly seen. Moreover, the reduced accumulation rate for materials with higher initial thermal conductivity is also seen. Additionally, work by Kelly [23] on nuclear graphite materials (Pile Grade A and Gilsocarbon) in the as-produced and 3400 °C annealed (thus increasing crystallite size and thermal conductivity) clearly indicates higher defect accumulation resistance for the pre-annealed, higher thermal conductivity materials.

As mentioned in the introduction, it has been previously shown that for ceramics such as alumina the accumulation of thermal defect resistance upon irradiation does not depend strongly on the initial conductivity (hence crystalline perfection) of the alumina studied. The high-purity polycrystalline alumina accumulated thermal defect resistance at approximately the same rate as single crystal alumina (sapphire) even though the thermal conductivities ranged from 18 W/m-K (polycrystal) to 42 W/m-K (single crystal). It is apparent that graphite does not behave in this manner.

The behavior of the thermal defect accumulation in graphite discussed above can be explained in terms of accumulation of simple defects during irradiation. As mentioned in the introduction, the primary defects responsible for thermal conductivity reduction at these irradiation temperatures are lattice vacancies and simple complexes of interstitials and vacancies. In the work by Taylor [6] the actual concentration of vacancies was calculated based on phonon transport theory and an experimental program of irradiation and annealing. In this way Taylor determined the concentration of vacancies for pyrolytic graphite irradiated at ~450 °C to a fluence about twice that of the present study to be ~0.49%. The vacancy concentrations for the lower temperature irradiations in the Taylor study were considerably higher due to the reduced mobility of migrating defects suppressing the annihilation of defects produced following a fast neutron-induced cascade. Moreover, the interstitial defect contribution was shown by Taylor to be insignificant above ~300 °C. Kelly [1] and others have concluded that the thermal resistance due to vacancies is directly proportional to vacancy concentration. The thermal defect resistance plots (Figs. 6–8) could then be considered to be directly proportional to the vacancy concentrations of the material. However, this assumes an accumulation of a single type (size) of vacancy complex.

The initial accumulation of thermal defect resistance is considerably higher for materials with lower initial thermal conductivity and can be attributed to migration of interstitials and annihilation of vacancies following the atomic displacement cascade. It is reasonable to assume that materials with lower conductivity possess lower crystalline perfection and smaller crystallites and that this retards the migration of interstitials. Limiting the migration of interstitials would lead to less recombination and a higher saturation vacancy concentration. The reason for the transition to a linear accumulation of thermal defect resistance (cf Figs. 6–8) is less clear. As the irradiation dose increases the increased defect density will have the effect of both increasing the probability of annihilation of newly produced defects and increasing the complexity of the defects formed (i.e., larger, more stable vacancy loops.) The relative effectiveness of vacancies and loops on the thermal defect resistance can be described as follows [1]:

$$1/K_{RD} = (\alpha(x)/[\beta S_v^2 C_v + \Delta(C_{vloop}/r_0)],$$

where $1/K_{RD}$ and $\alpha(x)$ are as in Eq. (1), Δ is a numerical constant dependent on temperature, and β and S_v are constants. The defect variables are the defect radius r_0, and the vacancy and vacancy loop concentrations C_V and C_{vloop}, respectively. As discussed by Kelly [1], the vacancy term in Fig. 2 dominates thermal defect resistance below the 650–900 °C irradiation temperature with the loop term dominating at an irradiation temperature of 1350 °C.

A more detailed study of the nature and density of the vacancy complexes would be beneficial. However, it is interesting to note that in the classic work by Henson [24] the concentrations of the various defects prevalent for irradiation in the 300–650 °C irradiation temperature range were determined as a function of neutron fluence. For the Pile Grade A nuclear graphite of Henson's study the concentration of free vacancies accumulated in the same fashion as described in the present work. Moreover, other properties primarily effected by point-defect or simple defect clusters exhibit the same rapid rise and transition to linear accumulation. Specifically, the stored energy (Wigner energy, E_w) resulting from low-temperature neutron irradiation exhibits such behavior. In fact, Bell [25] has shown that the Wigner energy is directly proportional to the thermal defect resistance through the relationship $E_w = 6.25 (K_0/K_i - 1)_{30\ °C}$, or in terms of the thermal defect resistance $E_w = 6.25 (1/K_{RD})_{30\ °C}$. As pointed out by Kelly [1], the thermal defect resistance at low irradiation temperature is directly proportional to the vacancy concentration. The same is true for the accumulation of stored energy. Similarly, the elastic modulus of graphite, (which is dominated by the C44 elastic constant and related to the ability of graphite planes to shear over one another) is primarily affected by simple defect production. Such a correlation between elastic modulus change and thermal transport is to be expected. As pointed out by Taylor [5], the thermal transport in the basal plane can be directly related to the elastic constants C11 and C66. As with the stored energy, the rapid rise and deceleration of the change in elastic modulus is similar to the accumulation in thermal defect resistance shown here.

The previous discussion has avoided dealing with the material dependent constant $\alpha(x)$. This parameter, typically attributed to the porosity and other factors which increase the effective phonon path length through graphite, is generally in the range of .06–.2 for nuclear graphite and is less for materials with higher thermal conductivity. It is not clear to the author the best way to determine such a factor for a composite system where the thermal conduction is not necessarily equally shared between the fiber and matrix. However, finessing this question in no way alters the conclusions regarding the accumulation of thermal defect accumulation put forward. In fact, given that the constant is certainly lower for the composite materials as compared to the nuclear graphite H-451, the behavior of the accumulation of thermal defect resistance would be even more exaggerated than described above.

5. Conclusions

This work gives the first high-dose, in-situ, measurement of thermal conductivity for graphite materials. The data has been interpreted in terms of a thermal defect accumulation leading to the following conclusions which are reinforced by measurements in the literature taken by post-irradiation measurement of thermal conductivity. The thermal defect accumulation rate exhibits a significant, prompt rise rapidly making a transition to a lower, linear, accumulation rate. The initial accumulation of thermal defect resistance is related to the initial perfection of the material, with lower initial thermal conductivity materials exhibiting a larger initial accumulation rate. The behavior of the accumulation of thermal defect resistance is consistent with the dose behavior of the elastic modulus and stored energy, both of which are directly related to the simple point-defect accumulation.

References

[1] B.T. Kelly, The Thermal Conductivity of Graphite, in: P.L. Walker (Ed.), Chemistry and Physics of Carbon, vol. 5, Marcel Dekker, Inc., New York, 1969, p. 119.
[2] B.T. Kelly, Physics of Graphite, Applied Science Publishers, London, 1981.
[3] A. DeCombarieu, J. Phys. (France) 28 (1968) 931.
[4] R. Taylor, K.E. Gilchrist, L.J. Poston, Carbon 6 (1968) 537.
[5] R. Taylor, Philos. Mag. 13 (1966) 157.
[6] R. Taylor, B.T. Kelly, K.E. Gilchrist, J. Phys. Chem. Solids 30 (1969) 2251.
[7] J.W.H. Simmons, Radiation Damage in Graphite, 1st Ed., vol. 102, Pergamon, Berlin, 1965.
[8] L.L. Snead, T.D. Burchell, A.L. Qualls, J. Nucl. Mater. 321 (2003) 165.
[9] L.L. Snead, Fusion Energy Application, in: T.D. Burchell (Ed.), Carbon Materials for Advanced Technologies, Elsevier Science Ltd, Kidlington, Oxford, England, 1999, p. 389.
[10] C.R. Kennedy, E.M. Woodruff, Irradiation Effects on the Physical Properties of Grade TSX Graphite, Westinghouse Hanford Company, 1989.

[11] V. Barabash, L.L. Snead, J. Nucl. Mater. 329–333 (2004) 860.
[12] L.L. Snead, T.D. Burchell, Reduction in Thermal Conductivity Due to Neutron Irradiation, 22nd, 1995, San Diego, CA.
[13] L. Binkele, J. Non-Equilib. Thermodynam. 3 (1978) 257.
[14] B.T. Kelly, Carbon 9 (1971) 783.
[15] T.D. Burchell, W. P. Eatherly, J. P. Strizak, Effects of Radiation on Materials: 16th International Symposium, ASTM STP 1175, 1994.
[16] L.L. Snead, T.D. Burchell, J. Nucl. Mater. 224 (1995) 222.
[17] C.H. Wu, J.P. Bonal, B. Thiele, J. Nucl. Mater. 212–215 (1994) 1168.
[18] J.P. Bonal, C.H. Wu, J. Nucl. Mater. 228 (1996) 155.
[19] B.A. Thiele, et al., in: Proceedings of 16th International Symposium on Effects of Radiation on Materials, ASTM, 1992.
[20] L.L. Snead, S.J. Zinkle, D.P. White, J. Nucl. Mater. 340 (2005) 187.
[21] R.J. Price, General Atom. (1974).
[22] G.B. Engle et al., General Atom. (1974) 73.
[23] B.T. Kelly, P. Schofield, R.G. Brown, Carbon 28 (1990) 155.
[24] R.W. Henson, A.J. Perks, J.W.H. Simmons, Carbon 6 (1968) 789.
[25] J.C. Bell et al., Philos. Trans. Roy. Soc. A 254 (1962) 361.